Cell Reports
Physical Science

CellPress
OPEN ACCESS

Article

# Enhancement of ion diffusion by targeted phonon excitation

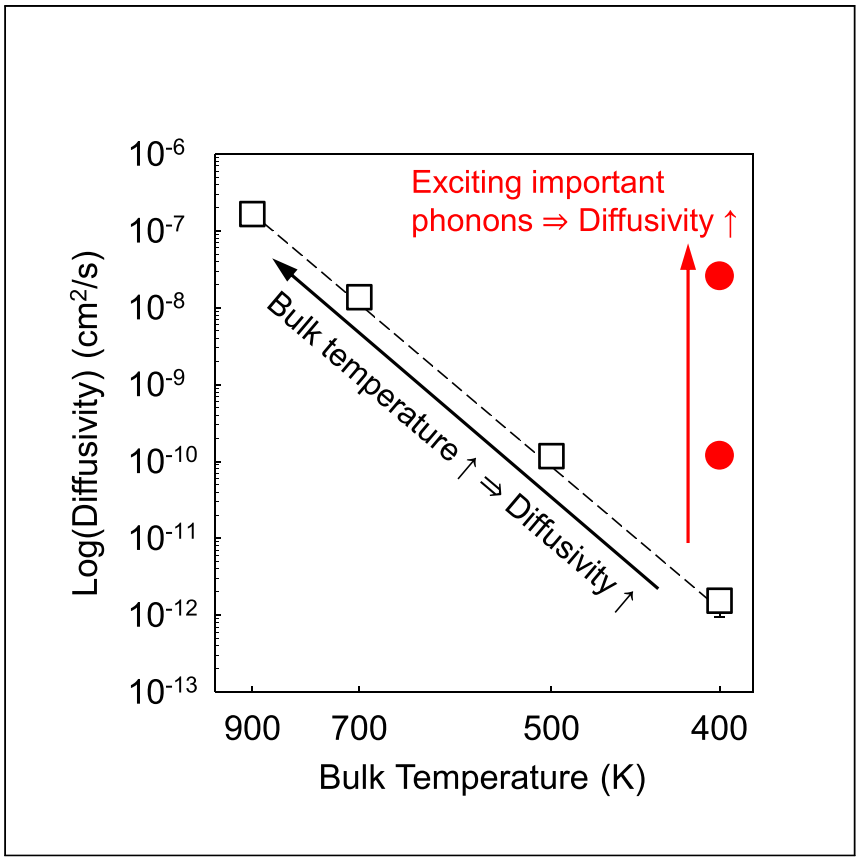


Gordiz et al. computationally show that, by exciting the top contributing phonons to the ion hop, diffusivity increases without raising the bulk temperature. This observation suggests that diffusion,or more generally any transition, can be enhanced by exciting only the contributing phonons to that transition to elevated temperatures, instead of heating up the entire material.

Kiarash Gordiz, Sokseiha Muy, Wolfgang G. Zeier, Yang Shao-Horn, Asegun Henry

kgordiz@mit.edu (K.G.)
ase@mit.edu (A.H.)

## Highlights

Computationally detecting the contributing phonons to the ion hop in solids

Identifying the important phonons in the $Li^+$ diffusion in Ge-doped $Li_3PO_4$

Targeted phonon excitation raises diffusivity without raising the bulk temperature

Avenue for increasing diffusivity by phonon engineering without changing chemistry

Gordiz et al., Cell Reports Physical Science 2, 100431
May 19, 2021 
https://doi.org/10.1016/j.xcrp.2021.100431

Cell Reports
Physical Science

CellPress
OPEN ACCESS

Article

# Enhancement of ion diffusion by targeted phonon excitation

Kiarash Gordiz,[1,*] Sokseiha Muy,[2] Wolfgang G. Zeier,[3] Yang Shao-Horn,[1,2,4] and Asegun Henry[1,5,*]

## SUMMARY

**Ion diffusion is important in a variety of applications, yet fundamental understanding of the interaction of phonons and the mobile species in solids is still missing. In this work, we introduce two formalisms that determine the individual contributions of phonons to the diffusion of ions through a solid, based on nudged elastic-band calculations and molecular dynamics simulations. The results for a model ion conductor of Ge-substituted $Li_3PO_4$ ($Li_{3.042}Ge_{0.042}P_{0.958}O_4$) reveal that more than 87% of the $Li^+$ ion diffusion originates from less than 10% of the vibrational modes between 8 and 20 THz. By deliberately exciting a small, targeted subset of these contributing modes (<1%) to a higher temperature and still keeping the lattice at a low temperature, we observe an increase in diffusivity by several orders of magnitude. This new understanding identifies new avenues for increasing diffusivity by engineering the vibrations in a material without necessarily changing the compound chemistry.**

## INTRODUCTION

Solid state mass and ion diffusion is central to many applications, ranging from batteries[1] and fuel cells[2] to sensors[3] and filters.[4] In many of these applications, the performance is limited by the slow diffusion of mass or ions. Although some families of solid-ion conductors, such as silver iodide and $Li_{10}GeP_2S_{12}$ (LGPS) exhibit high ion conductivities of ~1 S/cm[5] and ~0.01 S/cm[6,7] at room temperature, respectively, achieving high ion conductivities for divalent ions, including oxides, is challenging. For the conductivity of oxygen ions exhibited by yttria-stabilized zirconia (YSZ)[8,9] to reach 0.01 S/cm, an elevated temperature of 1,100 K is needed. Higher oxygen diffusivity at a lower operating temperature could enable a lower system cost, longer life, and greater proliferation.[10] Great advances have been made to increase the ion transport by cation and anion substitution to alter the charge carrier density and the diffusion pathways to facilitate low-energy jumps. The classical approaches of chemical modification, such as cation and anion substitution, have led to tunable conductivity over several orders of magnitude in several families of super-ionic conductors, such as the lithium super-ionic conductor (LISICON)[7] and the sodium super-ionic conductor (NASICON).[11] Thus, regardless of the mobile ion species, understanding the key factors that dictate ion conductivity is needed to devise new strategies to further increase the conductivity beyond tuning of chemical compositions.

One possible avenue to improve diffusivity without modifying the chemistry stems from considering the local ion movement in the structure. At a given temperature, ions thermally vibrate in their specific crystallographic lattice sites until sufficient thermal energy is available for an ion jump. The coupled ion vibration and ion movement that is paramount for ion diffusion leads to the idea that lattice vibrations

[1]Department of Mechanical Engineering, Massachusetts Institute of Technology, Cambridge, MA 02139, USA

[2]Department of Materials Science and Engineering, Massachusetts Institute of Technology, Cambridge, MA 02139, USA

[3]Institute for Inorganic and Analytical Chemistry, University of Muenster, Corrensstr. 30, 48149 Münster, Germany

[4]Research Laboratory of Electronics, Massachusetts Institute of Technology, Cambridge, MA 02139, USA

[5]Lead contact

*Correspondence: kgordiz@mit.edu (K.G.), ase@mit.edu (A.H.)

https://doi.org/10.1016/j.xcrp.2021.100431

(phonons) may have a role in the ion jump. Such an idea can be further intuited by considering the role of temperature as a spectrum of scalar contributions, not as a single scalar value. Based on this more-detailed view, in solids and rigid molecules, temperature is composed of a summation of individual contributions by modes of vibration, which means that a group of vibrating atoms can be described as a summation of collective vibrations, each with a specific frequency, often termed eigen modes, normal modes, or phonons. According to the traditional description for solid-state diffusion based on the Arrhenius relation $D \propto \exp(-E_a/k_B T)$,[12] diffusivity increases exponentially with increasing temperature, where $k_B$ and $T$ denote the Boltzmann's constant and the bulk temperature, respectively. The term "bulk" temperature, here, denotes the temperature that would be sensed if the material were in thermal equilibrium. Although temperature is generally understood as a proxy for the level of excitation of the phonons or normal modes of vibration within a solid material, it should be noted that each mode has its own time-varying amplitude and individual temperature. It is possible for a material to experience some non-equilibrium in the individual mode temperatures, whereby certain modes are highly excited to an effective temperature above all others (e.g., joule heating of optical modes in a transistor[13]). In such a situation, a subset of modes can behave as though they are at a higher effective temperature than the bulk temperature.

In the classical limit, for an individual mode labeled $n$, the modal temperature $T_n$ is obtained from $k_B T_n = Q_n^2 \omega_n^2$, where $Q_n$ and $\omega_n$ are the modal displacement coordinates[14] (which can be interpreted as the mode amplitude) and frequency of vibration of mode $n$ (see Note S1 for a derivation of this relation and its quantum analog). The idea of modal temperatures have also been introduced in previous theoretical studies,[15] in which, for the first time, the two-temperature model was extended to study the weak coupling between certain groups of phonons and its effect on thermal transport in solid materials. Our focus in this study is the distinction between the bulk and modal temperatures and how that influences solid-state ion transport. As the bulk temperature increases, the amplitudes of all the modes in the system increase, which facilitates ions to hop over activation barriers, thereby enhancing diffusion. There are practical ways, however, to increase the amplitude and temperature of a small subset of normal modes by exciting them with light either directly through photon-phonon coupling[16–19] or indirectly through electron-photon coupling[20–22] or THz electric fields[23] and keeping them in non-equilibrium with respect to the rest of the modes, without increasing the bulk temperature. This idea of selective vibrational mode excitation has been used in previous studies, as a novel tool, to modify the electronic properties of the structure through electron-phonon coupling for plasmonics,[24] photovoltaics,[25,26] and charge-transport applications.[27] Selective modal excitations have also been used to induce vibrational and structural changes in the system for phase-change applications.[28,29] Inspired by recent experimental observation of solid-state ion-diffusion induced by external THz-electric field illumination,[23] in this study, we aim to examine whether only a small subset of modes in the lattice are responsible for the hopping of ions, which would allow the increase of the diffusivity by exciting those subset of modes without increasing the bulk temperature. Experimental realization of such an idea would have far-reaching implications for chemical reactions, phase transitions, or other related phenomena because it would suggest that migration along a reaction/transition coordinate could be accelerated by exciting only the most important normal modes, rather than all the modes via an increase in the bulk temperature. This approach would mean that a material and its container could remain "cold," but it could exhibit kinetics associated with a much higher temperature, by only making a subset of the most important modes "hot." To assess that opportunity, we use the example of ion diffusion, in which we

(1) identify the mode-level contributions to ion diffusion to determine how many modes are responsible for an ion hop in the system, and (2) quantify to what extent diffusivity can be increased by targeted excitation of a small subset of these contributing modes without increasing the bulk temperature.

The role of specific structural modes and phonons in facilitating solid-state diffusion has been reported in other studies.[30–41] The frequency of longitudinal acoustic phonons was shown to exhibit a strong correlation with the enthalpy of self-diffusion in body-centered cubic metals.[33] In addition, octahedral rotation has been shown to promote fast oxygen-ion conduction in perovskite-related phases.[30,31,35,39,40] Li and Benedek[37] calculated the force constants associated with octahedral rotations in different Ruddlesden-Popper phases and showed that the willingness of a material to go under these octahedral rotations correlates with the migration barrier of oxygen ions. Similarly, anion rotation in closo-borate solid electrolytes has been shown to be important for ion transfer through the lattice.[32,36,41] Recently, Muy et al.[38] showed that lowering the computed average vibrational frequency of the lithium sublattice in LISICON by cation and anion substitution is accompanied by a reduced migration barrier. Similar correlations between activation energy and computed average frequency of sodium ions have been noted for sodium ion conductors,[34] in which activation energy is correlated with the Debye temperature, a proxy for the softness of the lattice, i.e., corresponding to low-energy vibrational modes. However, the average frequency of vibration reflects a weighted sum over all phonon modes, and the Debye temperature only measures the slopes of the acoustic phonon modes at very low wave vectors, neglecting the influence of the optical phonons and including the effect of some irrelevant phonons to ion migration. Most of these insights have been obtained from density-functional theory (DFT) lattice relaxation, *ab initio* molecular dynamics (AIMD), or experimental characterization. However, no direct information about specific phonons and their respective eigenvectors have been employed in a systematic way to obtain a deeper insight into these phenomena. The information for eigenvectors of phonons have been used in several modal-analysis methodologies for thermal transport, including atomistic Green's function (AGF),[42] Boltzmann transport equation (BTE),[43] and molecular dynamics (MD) simulations.[44–47] These methods have shown that, in different materials, certain groups of modes could contribute to heat transfer with higher rates, for instance, the high-frequency, in-plane phonons in graphene[48] and interfacial modes in semiconductor interfaces.[49–51] In this study, we aimed to identify modes of vibration that facilitate the ion migration by directly using the knowledge of phonons and their respective eigenvectors, based on the approaches that were recently developed in the context of MD-based phonon analysis.[44–47]

Here, we chose Ge-substituted $Li_3PO_4$ as our model system because $Li_3PO_4$ is a well-known parent structure; from which, numerous fast, solid conductors have been developed, including LGPS,[52,53] and its ion conductivity can be tuned up to ~10 orders of magnitude by aliovalent and anion substitution.[6] To identify the modal contributions to the diffusion of the lithium ion, which is the only diffusing species in the structure, we introduce two methodologies, one based on nudged elastic band (NEB) calculations and another based on MD simulations. Following the previously developed approaches for modal decomposition of thermal transport,[44–47] we project the atomic displacement or velocity fields onto the normal modes of vibration along the hopping trajectory obtained from a NEB calculation. The magnitude of the projection determines which phonons/normal modes become excited to facilitate that specific ion hop. Our results suggest that only a small subset of the phonons is responsible for ion diffusion in Ge-substituted $Li_3PO_4$ and that diffusivity can be

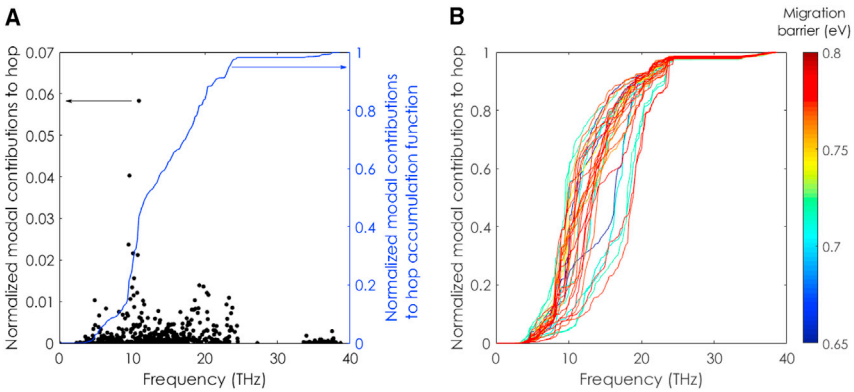


**Figure 1. Modal contributions to the ion hops in our model Ge-substituted $Li_3PO_4$ structure**

(A) Modal contributions in the form of scattered (black dots) and accumulation (blue line) plots for one individual Li ion hop; the energy of each mode is normalized by the lattice energy in that snapshot

(B) Modal contributions in accumulation plots for all 619 detected hops in our model Ge-substituted $Li_3PO_4$ structure. Because of the broken symmetry, different pathways in the system will theoretically have different migration barriers; the distribution of which is shown by different colors.

increased by increasing only the temperature of those modes instead of the bulk temperature.

## RESULTS AND DISCUSSION

### Modal contributions obtained from NEB calculations of Ge-substituted $Li_3PO_4$

The modal contributions to one example hop in Ge-substituted $Li_3PO_4$ shows that a small subset of modes (around 10 THz) contributed much greater than the rest of the modes (Figure 1A). The dominant hopping mechanism in the Ge-substituted $Li_3PO_4$ structure, is the concerted hop[54] of two Li ions, one of which is the interstitial, as shown in Figure 2C, and it is compared with two other hopping mechanisms in Figures 2A and 2B. The concerted hop mechanism is known as the interstitialcy mechanism,[55,56] which has been reported[57,58] as the dominant mechanism for lithium ion diffusion in $Li_3PO_4$ and is used as the migration mechanism for the NEB-based modal analyses presented in this study. The normalized integrations of the contributions with respect to frequency (the accumulation) are shown as a continuous curve in Figure 2B for all the 619 hops in the structure (the process of identifying those hops is explained in the Experimental procedures section). Most of the contributions to all the hops in the system come from modes between 8 and 20 THz (Figure 1B). Although that range is centered around the attempt frequency of the lithium ion (~14 THz; see Figure S1 and Note S2 for the calculation procedure), the large range of frequencies for the contributing phonons shows that more-intricate phonon processes are operative, which differs from the simpler picture described by traditional approaches,[59] wherein only one value of vibrational frequency (the attempt frequency) enters the formulation. By averaging over all the modal contributions calculated for all the hops in the system (Figures S2), we confirmed that, on average, >87% of the lattice energy during the ion hop in the structure came from <10% of the modes in the system (Figure S3). In addition, as is explained and shown in Figure S4, in each hopping event, there is at least one mode that has a contribution more than 10 times the average contribution by all the modes. Thus, the results in Figure 1 show that in Ge-substituted $Li_3PO_4$, only a few modes are responsible for the interstitialcy diffusion mechanism in Figure 2C.

Because of the larger vibration amplitudes that localized modes attribute to the interstitial and other neighboring ions than that of the delocalized modes[60]

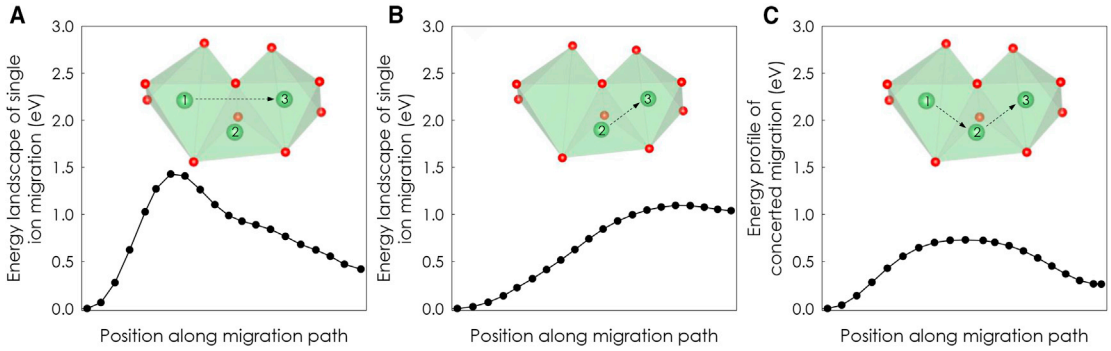


**Figure 2. Three hopping mechanisms in Ge-substituted $Li_3PO_4$ structure and the energy along the MEP (dotted curves) obtained from NEB calculations**

(A) The direct hop of a Li ion forming an octahedral (interstitial) at site (1) to another unoccupied octahedral site 3.

(B) The hop of a Li ion from a tetrahedral (lattice) site 2 to an unoccupied octahedral site 3.

(C) The concerted hop of two Li ions, in which one hops from a tetrahedral site 2 to an unoccupied octahedral site 3, and the other hops from an octahedral site 1 to the tetrahedral site that was previously occupied by the first Li ion (site 2). The dominant hopping mechanism in Ge-substituted $Li_3PO_4$ structure, is the concerted hop of two Li ions because of its lower migration barrier (MB) than the other two mechanisms.

(Figure 3), localized modes might be the most strongly contributing modes to each ion hop. However, inspection of the eigenvectors for the top two contributing modes in Figure 1A (at 9.64 THz and 10.94 THz) revealed that highly contributing modes can be either delocalized (Figure 3A) or localized (Figure 3B) in nature. Because the modal analysis formalism is based on the supercell lattice dynamics (SCLD) calculations (see Experimental procedures), all types of vibrational modes in the system with no inherent assumptions about their character were identified; from which, the contributions to ion diffusion, even for localized modes, were computed. Having access to such a formalism (see Experimental procedures) is crucial because, by breaking the symmetry in the system (e.g., by inclusion of vacancies and interstitial and substitutional ions, which is common in highly conductive solid electrolytes[61]), the conventional picture of propagating phonons in pure crystalline solids breaks down as other non-propagating and localized modes must be included.[50,62,63] Figure S6 shows the spectral distribution of all the localized modes of vibration for all the equilibrium configurations in our Ge-substituted $Li_3PO_4$.

## Diffusivity enhancement by excitation of the highly contributing modes

Figure 4 shows that increasing the energy of the top five contributing modes among all the possible hops belonging to the equilibrium configuration present at each time step during an MD simulation—by increasing their temperature to 500 K and 700 K—increases the diffusivity by 2 ($\sim 10^{-10}$ $cm^2/s$) and 4 ($\sim 10^{-8}$ $cm^2/s$) orders of magnitude respectively, compared with its value ($\sim 10^{-12}$ $cm^2/s$) in the unperturbed (natural) simulation at a lower temperature of 400 K. In fact, when the lattice is kept at 400 K and only the top five most-contributing modes are excited to a particular temperature, the diffusivity becomes what it would have been if the entire material had been heated to that temperature. Unexpectedly, even if we excite only the single highest-contributing mode in each of the equilibrium configurations, almost the same increase in the diffusivity is observed. The small difference between the increase in diffusivity by exciting the five highest-contributing modes and the one by exciting only the highest-contributing mode can be explained by noting that more kinetic energy is input to the hopping ion by exciting five modes. How these excited modes interact with the rest of the unexcited modes in the system is an interesting topic for a future study, which can be investigated using the two-temperature model that was presented in a recent study.[15]

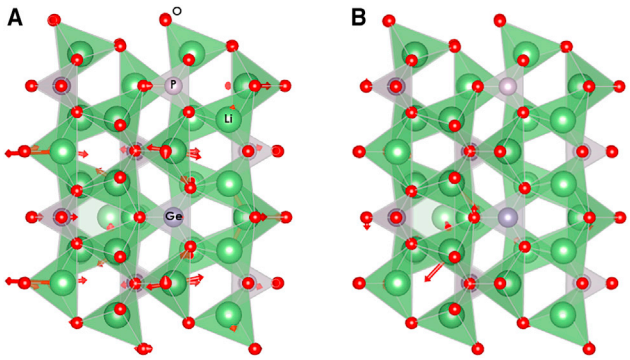


**Figure 3. Comparison between the eigenvectors of vibration belonging to the top two contributing modes to the ion hop in the Ge-substituted $Li_3PO_4$ structure**

Eigenvectors of vibration are shown by red arrows and are considered for the (A) highest and (B) second-highest contributing modes in Figure 1A. Eigenvectors follow a (A) uniform and (B) non-uniform distribution, which correspond to the delocalized and localized nature of these depicted modes, respectively. The chosen equilibrium atomic configuration corresponds to panel 6 in Figure S5.

To illustrate that the increase in diffusivity from excitation only happens when the specific modes that matter most are excited, Figure 4 shows that exciting five random modes in the 8–20 THz frequency range did not lead to significant enhancement in the diffusivity. The novelty of discovering that only a small subset of vibrational modes is responsible for the orders-of-magnitude increase in diffusivity by modal excitation can be understood by noting the theoretical definition of the diffusion coefficient in solid materials, $D = D_0 \exp\left(-E_A/k_B T\right)$.[59] In that definition, $E_A$ and $D_0$ are known as the activation energy and the prefactor. According to the transition state theory,[64] $E_A$ and the passing of an ion through the transition state are solely influenced by one mode of vibration in the system. However, $D_0$ is theoretically influenced by many modes of vibration in the system, which can be understood by noting its dependence on several other parameters, $D_0 \propto a^2 n\nu \exp\left(\Delta S_m/k_B\right)$, where $a$, $n$, $\nu$, and $\Delta S_m$ are the lattice constant, the number of the nearest hopping sites, the average frequency of vibration for the hopping atom, and the entropy of migration, respectively. Among these parameters, $\Delta S_m$ is a function of all the frequencies of vibration in the system, and because of its exponential influence, it can affect the diffusion coefficient by orders of magnitude, to a degree comparable to the influence of the migration barrier, as was shown in recent studies by Krauskopf et al.[34] and Muy et al.[65] Therefore, because, theoretically, many modes of vibration influence $\Delta S_m$, and hence, $D_0$, the observation that by exciting only a few modes in the system, the diffusivity can change by several orders of magnitude, is, indeed, unexpected.

To check whether traditional parameters for diffusivity[66] can explain the enhanced diffusion rates caused by modal excitation in Figure 4, we quantified the changes in attempt frequency (Figure S1), jump rate (Table S1), radial distribution function (RDF) (Figure S7), amplitude of vibration (Figure S8), Haven ratio (the ratio of the tracer diffusion coefficient to the conductivity [total] diffusion coefficient,[67] which can be interpreted as an index for the strength of correlated hops in the system) (Table S2), and the migration barrier (Figure S9). However, the very small changes in those parameters were not able to explain the orders-of-magnitude increase in diffusivity observed by modal excitation (Figure 4). This also highlights the novelty of the mechanism discovered herein, illustrating the importance of modal temperatures

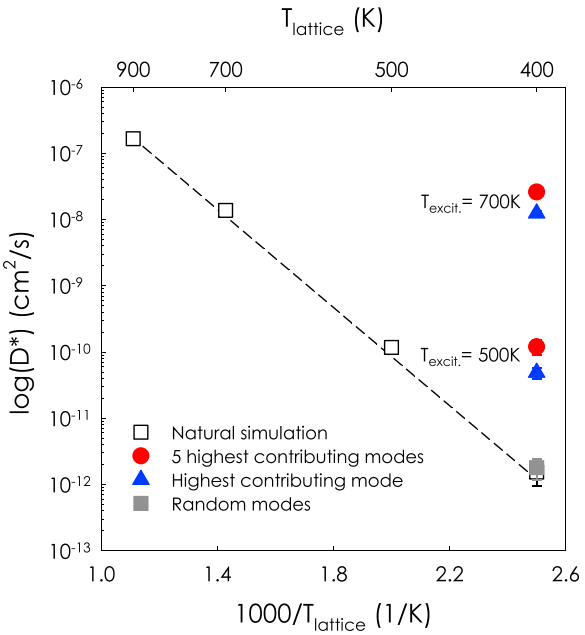


**Figure 4. Effect of targeted phonon excitation on the ion diffusion in the Ge-substituted $Li_3PO_4$ structure**

By exciting the five highest-contributing modes or even the single highest-contributing mode to ion diffusion in the Ge-substituted $Li_3PO_4$ structure to 500 K or 700 K and keeping the lattice at 400 K, the diffusivity increases by around two and four orders of magnitude compared with the unperturbed/natural simulation at 400 K. Exciting five random modes to 700 K, however, does not lead to a noticeable increase in diffusivity. The reported values are tracer diffusivity, but the same increase was also observed in the conductivity (total) diffusivity[67] (see Table S2). The activation energy obtained from the linear fitting of the Arrhenius equation[97] (0.68 eV) is in reasonable agreement with the one obtained from the NEB calculations for the interstitialcy hop (Figure 2). In addition, the orders of magnitude of our obtained diffusivity values are in agreement with the ones reported for similar structures in previous studies.[84,65] Error bars represent the standard deviation for each data point. For some data points, error bars cannot be seen because they are smaller than the marker size.

(i.e., modal energies) and the concept of directionality brought into the analysis by including the eigenvectors of vibration in our phonon-based methodologies (see Experimental procedures). Overall, the 2–4 orders-of-magnitude increase in diffusivity by modal excitation (Figure 4) can be attributed to increasing the energy of the highly contributing modes in the structure, and those modes can push the ion forward along its migration pathway. These results not only show that the identified modes of vibration using our proposed methodologies are correct and are indeed responsible for the ion diffusivity but also offer a new strategy to increase the diffusivity of known solid-state ionic conductors by using techniques such as direct[16,17,19] and indirect[20–22] coupling to phonons without increasing the temperature of the lattice.

## Modal contributions obtained from MD simulations of Ge-substituted $Li_3PO_4$

The modal contributions to the diffusivity for the Ge-substituted $Li_3PO_4$ structure, calculated from the mass diffusivity modal analysis (MDMA) method (see experimental procedures), are shown in Figure 5B. The increase in the diffusivity accumulation function in Figure 5B shows that the modes with frequencies between ~8 and 20 THz are responsible for ion diffusivity. This observation is in excellent agreement with the modal contributions obtained from the NEB-based approach (Figure 1B), which is also averaged and shown in Figure 5B. The accumulation of the partial

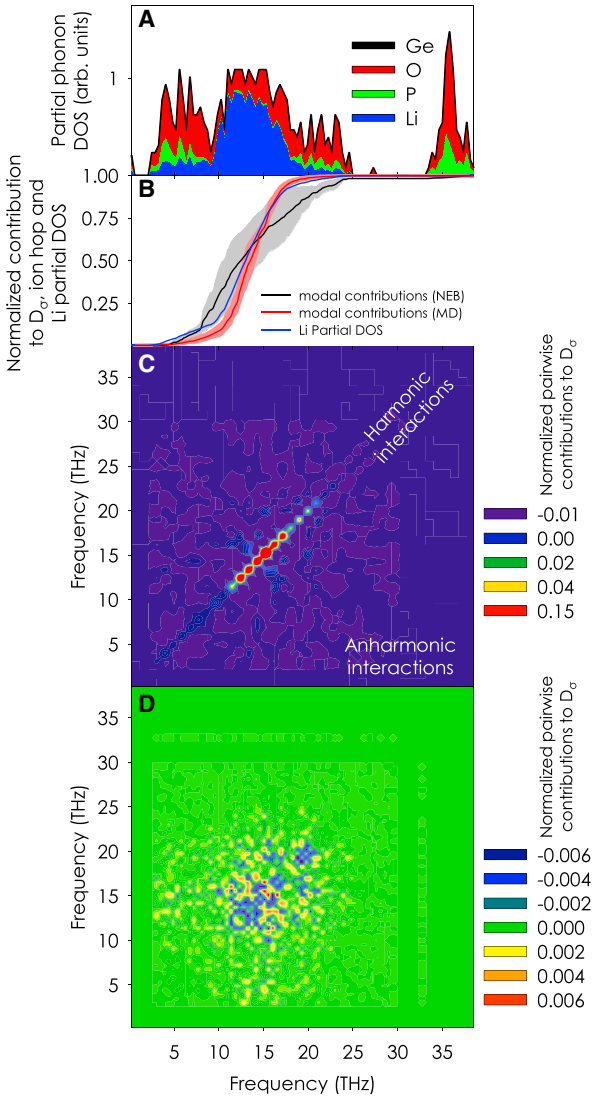


**Figure 5. Normalized modal contributions to the conductivity diffusivity in Ge-substituted $Li_3PO_4$ structure calculated from MD-based method (MDMA)**

The MDMA formalism is able to provide the degrees of both harmonic and anharmonic contributions to the ion diffusion in the lattice.

(A) Partial phonon DOS for different elemental components of the structure in the form of a stacked area chart.

(B) Modal contributions in the form of an accumulation function to the conductivity diffusivity obtained from the MDMA method (red curve) and to the ion hop from the NEB-based modal analysis (black curve). In addition, the accumulation function for the lithium partial DOS (blue curve) has also been shown.

(C) Two-dimensional (2D) map showing the magnitudes of the pairwise correlations/interactions contributing to the conductivity diffusivity on the plane of two frequency axes.

(D) Similar to (C), except the values on the diagonal (harmonic interactions) have been zeroed for better visualization of the off-diagonal terms (anharmonic interactions). The shaded gray and red regions in (B) represent the statistical distributions in NEB- (see Figure 1B) and MD-based modal decompositions, respectively. MD results shown on this plot are obtained from natural simulation at 800 K.

density of states (DOS) for lithium ions shown in Figure 5B, obtained from the partial DOS in Figure 5A, also shows reasonable agreement with the modal contributions obtained from the NEB-based and MDMA approaches. The generality of this

agreement should be investigated more in future studies; however, NEB and MDMA reveal the exact individual contributing modes to each ion hop in the system.

We use the MDMA formalism to, for the first time, quantify the anharmonic interactions that lead to ion diffusion in a solid lattice. Individual values of $D_{\sigma,n,n'}$ (see Equation 11 and the experimental procedures section) are shown on maps of correlation in Figures 5C and 5D. By summing over all the pairwise correlations in Figure 5C, we confirmed that >92% of the contributions to diffusivity arise from the correlations along the diagonal (iso-frequency modes), indicating that most of the contributions by phonons to the diffusivity in the Ge-substituted $Li_3PO_4$ system originate from the harmonic interactions. The remaining contributions (~8%) came from off-diagonal terms (anharmonic interactions), which can be observed better in Figure 5D after omitting the diagonal terms (i.e., artificially setting them to zero). Even after removing the diagonal terms, all the large contributions are still close to the diagonal, which shows that all the anharmonic terms are also between the modes that have relatively similar frequencies. Quantifying anharmonic interactions is particularly important for fast ion conductors because the lower migration barriers in those ion conductors have been shown to be correlated with softer lattices,[34,38] which typically allow for greater degrees of anharmonic interactions.[68] In a recent study, using AIMD simulations and Raman polarization-orientation measurements, Brenner et al.[69] attributed the large broadening of vibrational peaks in AgI superionic conductor to the strong anharmonic interaction of the $Ag^+$ ion and the rigid iodine lattice. Our chosen Ge-substituted $Li_3PO_4$ compound is not a superionic conductor, which could be the reason for the low degrees of anharmonic contributions that we calculated for ion conduction from the MDMA method. Overall, our analysis provides a quantitative way to measure the effect of anharmonicity on the solid-state diffusion, which has already been recognized in earlier works, but little quantitative evidence has been provided,[70,71] and that is, with the exception of a few compounds, such as $CuCrSe_2$[72] and $AgCrSe_2$,[73] where recently, inelastic neutron-scattering measurements have revealed a softening of acoustic modes, which are associated with the superionic transitions in those materials. Ultimately, more studies are needed to compare the inelastic interactions observed for our Ge-substituted $Li_3PO_4$ compound with other ion conductors with more-polarizable anions in which the anharmonicity is expected to be more important.[74,75]

We have introduced two modal decomposition formalisms (see experimental procedures) that determine the individual normal mode contributions to ion diffusion. Our results for a model structure of Ge-substituted $Li_3PO_4$ show that a small group of modes (<10% of the vibrational modes in the system) are responsible for >87% of the diffusion. Of greatest significance is that, when we externally excited a targeted subset of the highest-contributing modes, the diffusion increased to the value associated with the effective temperature of the targeted modes, even if the lattice is kept at a lower temperature. This observation is intriguing because a high diffusivity can be achieved while the bulk temperature of the material remains at a much lower temperature.

Although the selected Ge-substituted $Li_3PO_4$ composition in this study comprises a rather slow ion conductor, we think the presented, rigorous theoretical frameworks in this report can be used to study the fundamental concept of phonon-ion interaction, which is important in the field of superionics.[7,76–78] Recent reports have, so far, only linked the idea that phonons contribute to ion transport,[30–41] but this is the first study showing that specific-mode excitations can be used to influence diffusion in solids, which is influential to the field of lattice dynamics affecting ion transport

and will most likely lead to more work on optoionics.[79–81] In addition, the idea that a diffusion hop can be enhanced directly by phonon excitation has far-reaching implications. If such an effect can be confirmed experimentally (see Note S3 for a possible approach to experimental evaluation of the reported observations in this study), it would open the door to many new possibilities. For example, it may be possible to operate systems or devices that have portions that are diffusion limited at lower temperatures, which could lead to major cost savings and performance improvements. For instance, hypothetically, if oxygen diffusion through YSZ were limiting in solid oxide fuel cells (SOFCs), and the diffusivity it exhibits at a bulk temperature of 1,100 K could be achieved at a much lower temperature of 300–400 K, via some other means, there might be a dramatic effect on lowering the cost, enhancing the efficiency, and increasing the life and proliferation,[10] at the system level by using cheaper materials and seals for the piping/infrastructure. Furthermore, it is likely that this effect can be generalized to reactions, enabling a type of phonon catalysis,[82] whereby only the modes that matter are targeted and deliberately excited to accelerate a reaction. Similarly, this effect may be generalizable to phase transitions[28,29] and other transformations, or possibly even the reverse, i.e., the suppression of a reaction or phase transition by reducing the amplitude of the modes that facilitate the transition(s). The findings reported in this study, therefore, provide a gateway to thinking about new ways that specific vibrations can be used to enhance or potentially inhibit diffusion, reactions, and/or phase transitions, etc.

## EXPERIMENTAL PROCEDURES

### Resource availability

#### *Lead contact*

Further information and requests for resources should be directed to and will be fulfilled by the lead contact, Asegun Henry (ase@mit.edu).

#### *Materials availability*

This study did not generate new unique reagents.

#### *Data and code availability*

All data are available from the lead contact upon reasonable request.

### Modal decomposition based on NEB calculations

Ion diffusion in solids typically involves the translation of an ion from one location to another; in which, the starting and final locations usually correspond to ion configurations that are local minima in the potential energy surface (see Figure 6). Consequently, each of the equilibrium ionic configurations at the beginning and end of a hop could have a different set of normal modes of vibration. Thus, although we may have one minimum energy pathway (MEP) between equilibrium configurations 1 and 2 (see Figure 6), because of the different vibrational modes at these two energy minima, the modes that initiate an ion hop from site 1 to site 2 may be different from the ones that initiate a hop from site 2 to site 1. More explanation on how two different equilibrium configurations in one structure possess different normal modes of vibration is provided in Note S4. To determine which modes of vibration in a local equilibrium contribute to the ion hop along a specific pathway, we combine NEB and lattice dynamics (LD) calculations.

An NEB calculation[83] determines the MEP between two equilibrium configurations. Each NEB calculation results in a desired number of ionic configurations (snapshots of displaced ions) that are distributed along the MEP between the two end-equilibrium configurations. According to the LD formalism,[14] any atomic displacement field

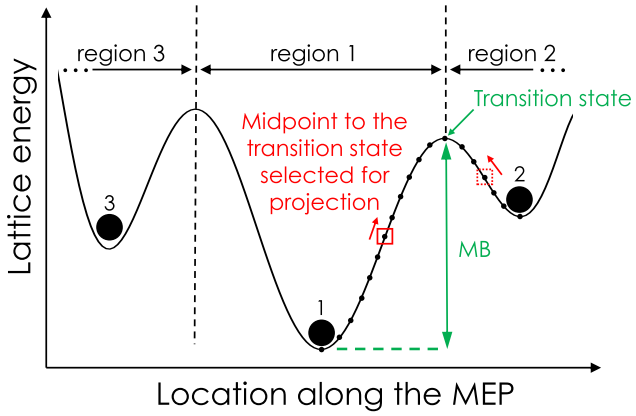


**Figure 6. MEP schematic between three minimum energy sites (sites 1, 2, and 3)**

Migration barrier (MB) is the maximum energy difference along the MEP (e.g., MB = $E_{\text{transition state}} - E_1$ for the hop from site 1 to site 2) that the hopping ion needs to overcome. The dots on the MEP between sites 1 and 2 show the ionic configurations (displacement fields) obtained from the NEB calculation. The displacement-field halfway points to the transition state, shown by the solid and dashed squares, are used to obtain the modal contributions to the ion hops from sites 1 to 2 and from sites 2 to 1, respectively.

can be projected onto any complete set of normal modes of vibration to determine how the normal modes superpose to recreate that exact displacement field. The magnitude of projection, as has been recently learned from modal decomposition of thermal transport,[44–47] shows the degree to which each normal mode is contributing to that displacement field, which can be quantified using the following expression,[14,47]

$$Q_n = \sum_{i=1}^{N} \sqrt{m_i}\mathbf{e}^*_{i,n} \cdot \mathbf{u}_i \qquad \text{(Equation 1)}$$

where $\mathbf{u}_i$ is the displacement of atom $i$ from its equilibrium position in the configuration at the hopping origin; $\mathbf{e}_{i,n}$ is the eigenvector for mode $n$, assigning the direction and displacement magnitude of atom $i$ obtained from an SCLD calculation[45,47,63] for the structure at the hopping origin; * denotes the complex conjugate operator; and $m_i$ is the mass of atom $i$. $Q_n$ is the modal displacement coordinate, the square of which is proportional to the mode potential energy $E_n$ according to Equation 2:

$$E_n = \frac{1}{2}\omega_n^2 Q_n^2 \qquad \text{(Equation 2)}$$

The total energy of the system $E$ is equal to the summation over all modal energy values, $E = \sum_n E_n$. Here, $E_n$ is the contribution by mode $n$ to the potential energy of the displaced lattice during the ion migration, which can be interpreted as the contribution by mode $n$ to the ion hop along its migration pathway. It should be noted that, in the presented NEB-based modal analysis, the definition for modal kinetic energy[14] could not be used as a metric for analyzing the modal contributions to the ion hop because the atomic velocities are not available in an NEB calculation. To perform the projection of the displaced atoms onto the normal modes, a choice must be made as to which configuration along the MEP should be used to perform the projection. Although that is somewhat arbitrary, for simplicity, we selected the configuration that is halfway between the hopping origin and the transition state (see Figure 6). We avoided projection on points closer to the saddle point based on the practical consideration that the structure would likely exhibit modes with imaginary frequencies near the transition state, which might introduce undesirable

complexity, the effect of which will be analyzed in follow-on studies. Nevertheless, we examined the projections closer to the beginning stages of the MEP, compared them to those at the halfway point, and noticed almost no change in the contributing modes (Figure S10), which suggests the choice of the halfway point is satisfactory, at least for the system under consideration. To calculate the modal contributions for all the possible hops in the structure, we applied the above procedure to (1) all the distinct equilibrium configurations in the system because each of them would have different vibrational modes, and (2) all the ion hops in each of those equilibrium configurations.

### NEB calculation details

To test our formulations, we chose Ge-substituted $Li_3PO_4$ as an example structure. The interatomic potentials for NEB calculations and MD simulations were obtained from a well-established form potential, which has been successfully tested in a number of previous studies,[65,84–87] including with Li-conducting compounds.[65,85] This form potential comprises a long-range coulomb term, a short-range Morse function, and a repulsive term. The parameters were obtained from the library of potentials developed by Pedone et al.,[88] which has been successfully tested in previous MD simulations of silicates and polyanion type materials, including $Li_3PO_4$.[84] The exact formulas and parameters of which are provided in Table S3. To further check the accuracy of this interatomic potential used, we calculated the lattice constants for the perfect $\gamma$-$Li_3PO_4$ crystal from the isobaric-isothermal MD relaxation at zero pressure and room-temperature and compared them with the existing first-principles[57] and experimental[89–91] values (Table S4). The comparison showed that the lattice constants in our simulations have <3% difference with other reported values. The pristine $Li_3PO_4$ structure was chosen to be a 3 × 2 × 1 supercell containing 192 atoms, ($\gamma$-$Li_3PO_4$, space group *Pnma*) with the lattice dimensions given is Table S4. In the pristine structure, one P was substituted by one Ge, and one Li was added in the form of an interstitial to maintain charge neutrality; hence, the structure contains 193 ions ($Li_{3.042}Ge_{0.042}P_{0.958}O_4$). This composition is a simple case to show the effectiveness of the modal excitation approach in this article. If the number of Ge-substitute atoms increases, for charge neutrality, the number of Li interstitials should also increase. More interstitial sites complicate the modal-excitation experiment because of the possibility of simultaneous hops in the simulation and the consequent challenge in deciding which modes to excite during the simulation. There are 36 available, unique interstitial sites to add this Li interstitial. However, among those 36 interstitial sites, only 31 resulted in a stable configuration with positive vibrational frequencies (Figure S5 shows schematics of those distinct configurations). Each hopping event brings the structure from one of those equilibrium configurations to another.

As is shown in the results section, the dominant hopping mechanism in our Ge-substituted $Li_3PO_4$ is the interstitialcy mechanism.[55,56] To determine the phonon contributions to all the possible interstitialcy hops in the system, we need to account for all the interstitialcy hops in each of the equilibrium configurations. To do so, we first counted the nearest-neighbor Li lattice sites to the interstitial ion. Then, for each of those nearest-neighbor Li lattice sites (tetrahedral sites), we counted the nearest-neighbor interstitial sites (octahedral sites), with the constraint that the nearest-neighbor interstitial site be among the 31 stable interstitial sites. Counting for all those combinations, resulted in 619 distinct hops in our structure that follow the interstitialcy mechanism. The SCLD calculations determined the normal modes of vibration for all 31 equilibrium configurations and were performed using the general utility lattice program (GULP)[92] package, whereas the MD simulations and the NEB

calculations were conducted using the large-scale atomic/molecular massively parallel simulator (LAMMPS)[93] package, following the formulations by Henkelman et al.[83] to ensure the correct determination of the saddle point. The reasons for why our calculations are based on classical interatomic potentials and LAMMPS package are discussed in Note S5.

### Targeted excitation of modes to enhance diffusivity

After finding the strongest contributing modes to the ion diffusion using the NEB approach, we examined whether external excitation of a small subset of those modes in an MD simulation had any measurable effect on the tracer and conductivity ion diffusivities. At each time step during the simulation, the equilibrium configuration was found by checking where the interstitial ion was located (i.e., which octahedral site was occupied) because the distinction between equilibrium configurations was based only on the occupied interstitial site and because the relative position of non-interstitial ions remained unchanged across different equilibrium configurations. By knowing the equilibrium configuration, we then excited the five highest-contributing modes among all the contributing modes to all the possible hops belonging to that configuration and kept the bulk temperature fixed. After a hop happened, a new equilibrium configuration was detected, and the process continued by exciting the five highest-contributing modes among all the possible hops associated with the new configuration.

Because ion diffusivity increases with temperature, we ensured that the bulk lattice temperature remained constant at a low temperature, so that any change in the diffusivity could be attributed only to the excitation of the targeted modes and not to the bulk temperature. To do so, we kept the total kinetic energy of the system constant via a velocity-rescaling scheme, in which, the addition of energy to the top five modes was complimented by a uniform reduction in the kinetic energy of all other modes in the system. To change the temperature of mode $n$ to a desired temperature $T_d$, we modified the atomic velocities in the system according to the following formula:

$$\mathbf{v}_i = \mathbf{v}_i + \frac{1}{\sqrt{m_i}}\left[\sqrt{2k_B T_d} - \dot{Q}_n(t)\right]\mathbf{e}_{i,n} \qquad \text{(Equation 3)}$$

where $\mathbf{v}_i$ is the velocity of atom $i$, and $\dot{Q}_n$ is the modal velocity coordinate defined by,[14]

$$\dot{Q}_n = \sum_{i=1}^{N} \sqrt{m_i}\mathbf{e}^*_{i,n} \cdot \mathbf{v}_i \qquad \text{(Equation 4)}$$

The derivation of Equation 3 is provided in Note S6. This rescaling procedure induces only a slight perturbation to the system, given that the top-five modes comprise only 0.86% of the modes in the system, and thus, the reduction in energy for all other modes is only <1% of their energy (see Note S7 and Table S5 for discussions about the needed thermalization power). In this study, the above-mentioned rescaling procedure was applied every five-times steps (every 5 fs). Although a velocity-perturbation scheme has been used in this study, other methods for modal excitation, such as atomic position perturbation[94] or simultaneous perturbation of atomic positions and velocities,[95] have also been employed in previous studies, particularly those with the goal of investigating the phonon-phonon interactions in MD simulations. However, the chosen method for modal excitation should not change the reported observations in this study because modal excitation (increasing the energy of a mode) can be achieved either by increasing the potential (position perturbation) or the kinetic (velocity perturbation) energy of the mode; the choice of which should not matter.

### Modal decomposition based on MD simulations

To directly obtain the contributing modes to the ion diffusion from MD simulations, we used the definition of diffusivity based on the fluctuation-dissipation theorem[96] and followed a modal-decomposition approach similar to that employed in MD-based thermal-transport studies.[44–47] Consistent with prior work on phonon transport,[44–47] we have termed this formalism "mass diffusivity modal analysis" (MDMA). In MDMA, the modal contributions to the atomic velocities are obtained and then used to decompose the following definition for conductivity diffusivity ($D_\sigma$):[67,75]

$$D_\sigma = \frac{N_c}{3}\int_0^\infty \langle \mathbf{v}_c(\tau)\mathbf{v}_c(0)\rangle d\tau \qquad \text{(Equation 5)}$$

Conductivity diffusivity ($D_\sigma$) not only includes the self-correlation information embedded in the tracer-diffusivity definition (Equation S11), but it also includes the many-particle-correlation information. In Equation 5, $N_c$ is the number of hopping particles in the system, $\langle\cdots\rangle$ denotes the auto-correlation operator, and $\mathbf{v}_c$ is the center of mass velocity for the hopping particles:

$$\mathbf{v}_c = \frac{1}{N_c}\sum_{i=1}^{N_c}\mathbf{v}_i \qquad \text{(Equation 6)}$$

To calculate the individual contribution by mode of vibration $n$ to $\mathbf{v}_i$ ($\mathbf{v}_{i,n}$), first modal velocity coordinate $\dot{Q}_n$ is calculated (Equation 4);[14] from which, $\mathbf{v}_{i,n}$ is determined by[14]

$$\mathbf{v}_i = \sum_{n=1}^{3N}\frac{\dot{Q}_n(t)}{\sqrt{m_i}}\mathbf{e}_{i,n} = \sum_{n=1}^{3N}\mathbf{v}_{i,n} \rightarrow \mathbf{v}_{i,n} = \frac{\dot{Q}_n(t)}{\sqrt{m_i}}\mathbf{e}_{i,n} \qquad \text{(Equation 7)}$$

Replacing $\mathbf{v}_i$ in Equation 6 with its modal contributions ($\mathbf{v}_{i,n}$) results in the modal contributions to the carriers' center of mass:

$$\mathbf{v}_c = \sum_{n=1}^{3N}\frac{1}{N_c}\sum_{i=1}^{N_c}\mathbf{v}_{i,n} \qquad \text{(Equation 8)}$$

which is substituted in one of the $\mathbf{v}_c$ terms in Equation 5 to extract the modal contributions to diffusivity ($D_{\sigma,n}$),

$$D_\sigma = \sum_{n=1}^{3N}\frac{1}{3}\int_0^\infty\left\langle\sum_{i=1}^{N_c}\mathbf{v}_{i,n}(\tau)\mathbf{v}_c(0)\right\rangle d\tau = \sum_{n=1}^{3N}D_{\sigma,n} \rightarrow D_{\sigma,n} = \frac{1}{3}\int_0^\infty\left\langle\sum_{i=1}^{N_c}\mathbf{v}_{i,n}(\tau)\mathbf{v}_c(0)\right\rangle d\tau \qquad \text{(Equation 9)}$$

Similarly, the modal contributions to ion conductivity ($\sigma_n$) can be obtained; the details of which are provided in Note S8.

By substituting for both center-of-mass velocities in Equation 5 with their modal contributions from Equation 7, the above formulations can be extended to capture the modal contributions to diffusivity in more detail:

$$D_\sigma = \sum_{n=1}^{3N}\sum_{n'=1}^{3N}\frac{1}{3}\int_0^\infty\left\langle\sum_{i=1}^{N_c}\mathbf{v}_{i,n}(\tau)\sum_{i'=1}^{N_c}\mathbf{v}_{i',n'}(0)\right\rangle d\tau = \sum_{n=1}^{3N}\sum_{n'=1}^{3N}D_{\sigma,n,n'} \qquad \text{(Equation 10)}$$

where individual contributions from the correlation/interaction of eigen mode pairs $n$ and $n'$ ($D_{\sigma,n,n'}$) are given by,

$$D_{\sigma,n,n'} = \frac{1}{3}\int_0^\infty\left\langle\sum_{i=1}^{N_c}\mathbf{v}_{i,n}(\tau)\sum_{i'=1}^{N_c}\mathbf{v}_{i',n'}(0)\right\rangle d\tau \qquad \text{(Equation 11)}$$

which provides additional insight into the degree to which each pair of modes interact, i.e., the anharmonicity via terms in which $n \neq n'$, to facilitate diffusion.

The combination of the MD- and NEB-based modal decomposition methods presented herein provides a detailed picture for the ion diffusion. Although both methods are based on projecting the trajectory of the hopping ion on the eigenvectors of vibration, the way they sample the phonon contributions to the ion hop is different. In the NEB-based approach, the contributions are calculated based on the atomic displacement field, whereas in the MD-based method, the contributions are obtained based on the atomic velocity field. In addition, MD samples the dominant mechanisms that are present in a natural simulation of the material, whereas NEB can be used to study specific mechanisms and the ion hop along specific migration pathways, regardless of the likelihood that they would occur at a given temperature.

### Diffusivity calculations

The total mean squared displacement method (TMSD) was used to measure the diffusivity of Li ions in our structure; the details of which are explained in the existing literature[97] and in Note S9. First, the structure was relaxed under the isobaric-isothermal ensemble for 1 ns at zero pressure and $T$ = 400 K and under the Nosé-Hoover canonical ensemble for another 1 ns at $T$ = 400 K; then, the structure was simulated for another 10 ns under the same ensemble to obtain the needed displacement data for diffusivity calculations. The time step was chosen to be 1 fs, and statistical uncertainty was reduced by considering five independent ensembles.[98] For calculating the conductivity-diffusion coefficients, total conductivity was calculated following the existing literarure;[67] the details of which are also explained in Note S9.

## SUPPLEMENTAL INFORMATION

Supplemental information can be found online at https://doi.org/10.1016/j.xcrp.2021.100431.

## ACKNOWLEDGMENTS

We acknowledge support from the National Science Foundation (NSF) career award to A.H. (award no. 1554050), the Office of Naval Research (ONR) under a MURI program (grant no. N00014-18-1-2429), and BMW.

## AUTHOR CONTRIBUTIONS

K.G., Y.S.-H., and A.H. conceived the idea. K.G. and A.H. derived the decomposition formulations. K.G. and S.M. performed the simulations. All authors contributed to the analyses, discussions, and writing of the manuscript.

## DECLARATION OF INTERESTS

Y.S.-H. is a board member at *Cell Reports Physical Science*. The remaining authors declare no competing interests.

Received: December 28, 2020
Revised: March 25, 2021
Accepted: April 20, 2021
Published: May 19, 2021

## REFERENCES


1. Takada, K. (2013). Progress and prospective of solid-state lithium batteries. Acta Mater. *61*, 759–770.
2. Jacobson, A.J. (2009). Materials for solid oxide fuel cells. Chem. Mater. *22*, 660–674.
3. Moseley, P. (1997). Solid state gas sensors. Meas. Sci. Technol. *8*, 223.
4. Gouaux, E., and Mackinnon, R. (2005). Principles of selective ion transport in channels and pumps. Science *310*, 1461–1465.
5. Turton, R. (2000). The Physics of Solids (Oxford University Press).
6. Bachman, J.C., Muy, S., Grimaud, A., Chang, H.H., Pour, N., Lux, S.F., Paschos, O., Maglia, F., Lupart, S., Lamp, P., et al. (2016). Inorganic solid-state electrolytes for lithium batteries: mechanisms and properties governing ion conduction. Chem. Rev. *116*, 140–162.
7. Kamaya, N., Homma, K., Yamakawa, Y., Hirayama, M., Kanno, R., Yonemura, M., Kamiyama, T., Kato, Y., Hama, S., Kawamoto, K., and Mitsui, A. (2011). A lithium superionic conductor. Nat. Mater. *10*, 682–686. https://doi.org/10.1038/nmat3066.
8. Malavasi, L., Fisher, C.A., and Islam, M.S. (2010). Oxide-ion and proton conducting electrolyte materials for clean energy applications: structural and mechanistic features. Chem. Soc. Rev. *39*, 4370–4387.
9. Skinner, S.J., and Kilner, J.A. (2003). Oxygen ion conductors. Mater. Today *6*, 30–37.
10. Scataglini, R., Mayyas, A., Wei, M., Chan, S.H., Lipman, T., Gosselin, D., D'Alessio, A., Breunig, H., Colella, W.G., and James, B.D. (2015). A total cost of ownership model for solid oxide fuel cells in combined heat and power and power-only applications. Lawrence Berkeley National Laboratory. April 22, 2016. https://www.energy.gov/sites/default/files/2016/06/f32/fcto_lbnl_total_cost_ownership_sofc_systems.pdf.
11. Fergus, J.W. (2012). Ion transport in sodium ion conducting solid electrolytes. Solid State Ion. *227*, 102–112.
12. Balluffi, R.W., Allen, S., and Carter, W.C. (2005). Kinetics of Materials (John Wiley & Sons).
13. Pop, E., Dutton, R.W., and Goodson, K.E. (2005). Monte Carlo simulation of Joule heating in bulk and strained silicon. Appl. Phys. Lett. *86*, 082101.
14. Dove, M.T., and Dove, M.T. (1993). Introduction to Lattice Dynamics (Cambridge University Press).
15. An, M., Song, Q., Yu, X., Meng, H., Ma, D., Li, R., Jin, Z., Huang, B., and Yang, N. (2017). Generalized two-temperature model for coupled phonons in nanosized graphene. Nano Lett. *17*, 5805–5810.
16. Först, M., Manzoni, C., Kaiser, S., Tomioka, Y., Tokura, Y., Merlin, R., and Cavalleri, A. (2011). Nonlinear phononics as an ultrafast route to lattice control. Nat. Phys. *7*, 854.
17. Li, X., Qiu, T., Zhang, J., Baldini, E., Lu, J., Rappe, A.M., and Nelson, K.A. (2019). Terahertz field-induced ferroelectricity in quantum paraelectric $SrTiO_3$. Science *364*, 1079–1082.
18. Morimoto, T., Nagai, M., Minowa, Y., Ashida, M., Yokotani, Y., Okuyama, Y., and Kani, Y. (2019). Microscopic ion migration in solid electrolytes revealed by terahertz time-domain spectroscopy. Nat. Commun. *10*, 2662.
19. Subedi, A., Cavalleri, A., and Georges, A. (2014). Theory of nonlinear phononics for coherent light control of solids. Phys. Rev. B Condens. Matter Mater. Phys. *89*, 220301.
20. Dekorsy, T., Cho, G., and Kurz, H. (2000). Light Scattering in Solids VIII (Springer-Verlag).
21. Dhar, L., Rogers, J.A., and Nelson, K.A. (1994). Time-resolved vibrational spectroscopy in the impulsive limit. Chem. Rev. *94*, 157–193.
22. Merlin, R. (1997). Generating coherent THz phonons with light pulses. Solid State Commun. *102*, 207–220.
23. Minami, Y., Ofori-Okai, B., Sivarajah, P., Katayama, I., Takeda, J., Nelson, K.A., and Suemoto, T. (2019). Ionic current in superionic conductor Na+ beta-alumina induced by terahertz electric fields. In Proceedings of the 44th International Conference on Infrared, Millimeter, and Terahertz Waves (IEEE), pp. 189–190.
24. Liu, J.G., Zhang, H., Link, S., and Nordlander, P. (2017). Relaxation of plasmon-induced hot carriers. ACS Photonics *5*, 2584–2595.
25. Ekins-Daukes, N., Ballard, I., Calder, C., Barnham, K., Trupke, T., Brown, A., Roberts, J., and Hill, G. (2003). Photovoltaic efficiency enhancement through thermal up-conversion. In Proceedings of the 3rd World Conference on Photovoltaic Energy Conversion, K. Kurokawa, L.L. Kazmcrski, B. McNelin, M. Yamaguchi, C. Wronski, and W.C. Sinke, eds. (IEEE), pp. 262–265.
26. Kim, J., and Kaviany, M. (2010). Phonon-coupling enhanced absorption of alloyed amorphous silicon for solar photovoltaics. Phys. Rev. B Condens. Matter Mater. Phys. *82*, 134205.
27. Bakulin, A.A., Lovrincic, R., Yu, X., Selig, O., Bakker, H.J., Rezus, Y.L., Nayak, P.K., Fonari, A., Coropceanu, V., Brédas, J.L., and Cahen, D. (2015). Mode-selective vibrational modulation of charge transport in organic electronic devices. Nat. Commun. *6*, 7880.
28. Hase, M., Fons, P., Mitrofanov, K., Kolobov, A.V., and Tominaga, J. (2015). Femtosecond structural transformation of phase-change materials far from equilibrium monitored by coherent phonons. Nat. Commun. *6*, 8367.
29. Itin, A., and Katsnelson, M. (2018). Efficient excitation of nonlinear phonons via chirped pulses: induced structural phase transitions. Phys. Rev. B *97*, 184304.
30. Chroneos, A., Parfitt, D., Kilner, J.A., and Grimes, R.W. (2010). Anisotropic oxygen diffusion in tetragonal $La_2NiO_{4+\delta}$: molecular dynamics calculations. J. Mater. Chem. *20*, 266–270.
31. Frayret, C., Villesuzanne, A., and Pouchard, M. (2005). Application of density functional theory to the modeling of the mixed ionic and electronic conductor $La_2NiO_{4+\delta}$: Lattice relaxation, oxygen mobility, and energetics of frenkel defects. Chem. Mater. *17*, 6538–6544.
32. Hanghofer, I., Gadermaier, B., and Wilkening, H.M.R. (2019). Fast rotational dynamics in argyrodite-type $Li_6PS_5X$ (X: Cl, Br, I) as seen by $^{31}P$ nuclear magnetic relaxation—on cation-anion coupled transport in thiophosphates. Chem. Mater. *31*, 4591–4597.
33. Köhler, U., and Herzig, C. (1988). On the correlation between self-diffusion and the low-frequency LA $^2/_3$<111> phonon mode in b.c.c. metals. Philos. Mag. A Phys. Condens. Matter Defects Mech. Prop. *58*, 769–786.
34. Krauskopf, T., Muy, S., Culver, S.P., Ohno, S., Delaire, O., Shao-Horn, Y., and Zeier, W.G. (2018). Comparing the descriptors for investigating the influence of lattice dynamics on ionic transport using the superionic conductor $Na_3PS_{4-x}Se_x$. J. Am. Chem. Soc. *140*, 14464–14473.
35. Kushima, A., Parfitt, D., Chroneos, A., Yildiz, B., Kilner, J.A., and Grimes, R.W. (2011). Interstitialcy diffusion of oxygen in tetragonal $La_2CoO_{4+\delta}$. Phys. Chem. Chem. Phys. *13*, 2242–2249.
36. Kweon, K.E., Varley, J.B., Shea, P., Adelstein, N., Mehta, P., Heo, T.W., Udovic, T.J., Stavila, V., and Wood, B.C. (2017). Structural, chemical, and dynamical frustration: origins of superionic conductivity in closo-borate solid electrolytes. Chem. Mater. *29*, 9142–9153.
37. Li, X., and Benedek, N.A. (2015). Enhancement of ionic transport in complex oxides through soft lattice modes and epitaxial strain. Chem. Mater. *27*, 2647–2652.
38. Muy, S., Bachman, J.C., Giordano, L., Chang, H.H., Abernathy, D.L., Bansal, D., Delaire, O., Hori, S., Kanno, R., Maglia, F., et al. (2018). Tuning mobility and stability of lithium ion conductors based on lattice dynamics. Energy Environ. Sci. *11*, 850–859.
39. Parfitt, D., Chroneos, A., Kilner, J.A., and Grimes, R.W. (2010). Molecular dynamics study of oxygen diffusion in $Pr_2NiO_{4+\delta}$. Phys. Chem. Chem. Phys. *12*, 6834–6836.
40. Villesuzanne, A., Paulus, W., Cousson, A., Hosoya, S., Le Dréau, L., Hernandez, O., Prestipino, C., Houchati, M.I., and Schefer, J. (2011). On the role of lattice dynamics on low-temperature oxygen mobility in solid oxides: a neutron diffraction and first-principles investigation of $La_2CuO_{4+\delta}$. J. Solid State Electrochem. *15*, 357–366.
41. Zhang, Z., Roy, P.-N., Li, H., Avdeev, M., and Nazar, L.F. (2019). Coupled cation-anion dynamics enhances cation mobility in room-temperature superionic solid-state electrolytes. J. Am. Chem. Soc. *141*, 19360–19372. https://doi.org/10.1021/jacs.9b09343.
42. Sadasivam, S., Che, Y., Huang, Z., Chen, L., Kumar, S., and Fisher, T.S. (2014). The atomistic Green's function method for interfacial phonon transport. Annu. Rev. Heat Transf. *17*, 89–145.

43. Esfarjani, K., Chen, G., and Stokes, H.T. (2011). Heat transport in silicon from first-principles calculations. Phys. Rev. B Condens. Matter Mater. Phys. *84*, 085204.

44. Gordiz, K., and Henry, A. (2015). A formalism for calculating the modal contributions to thermal interface conductance. New J. Phys. *17*, 103002.

45. Gordiz, K., and Henry, A. (2016). Phonon transport at interfaces: determining the correct modes of vibration. J. Appl. Physiol. *119*, 015101.

46. Lv, W., and Henry, A. (2016). Direct calculation of modal contributions to thermal conductivity via Green-Kubo modal analysis. New J. Phys. *18*, 013028.

47. Seyf, H.R., Gordiz, K., DeAngelis, F., and Henry, A. (2019). Using Green-Kubo modal analysis (GKMA) and interface conductance modal analysis (ICMA) to study phonon transport with molecular dynamics. J. Appl. Physiol. *125*, 081101.

48. Wu, X., and Luo, T. (2014). The importance of anharmonicity in thermal transport across solid-solid interfaces. J. Appl. Physiol. *115*, 014901.

49. Chalopin, Y., and Volz, S. (2013). A microscopic formulation of the phonon transmission at the nanoscale. Appl. Phys. Lett. *103*, 051602.

50. Gordiz, K., and Henry, A. (2016). Phonon transport at crystalline Si/Ge interfaces: the role of interfacial modes of vibration. Sci. Rep. *6*, 23139.

51. Zhou, Y., and Hu, M. (2017). Full quantification of frequency-dependent interfacial thermal conductance contributed by two-and three-phonon scattering processes from nonequilibrium molecular dynamics simulations. Phys. Rev. B *95*, 115313.

52. Kamphorst, J., and Hellstrom, E. (1980). Fast Li ionic conduction in solid solutions of the system $Li_4GeO_4$-$Li_2ZnGeO_4$-$Li_3PO_4$. Solid State Ion. *1*, 187–197.

53. Zhao, G., Suzuki, K., Yonemura, M., Hirayama, M., and Kanno, R. (2019). Enhancing fast lithium ion conduction in $Li_4GeO_4$–$Li_3PO_4$ solid electrolytes. ACS Appl. Energy Mater. *2*, 6608–6615.

54. He, X., Zhu, Y., and Mo, Y. (2017). Origin of fast ion diffusion in super-ionic conductors. Nat. Commun. *8*, 15893.

55. Chroneos, A., Yildiz, B., Tarancón, A., Parfitt, D., and Kilner, J.A. (2011). Oxygen diffusion in solid oxide fuel cell cathode and electrolyte materials: mechanistic insights from atomistic simulations. Energy Environ. Sci. *4*, 2774–2789.

56. Hayes, W., and Stoneham, A.M. (2012). Defects and Defect Processes in Nonmetallic Solids (Courier Corporation).

57. Du, Y.A., and Holzwarth, N. (2007). Li ion diffusion mechanisms in the crystalline electrolyte γ-$Li_3PO_4$. J. Electrochem. Soc. *154*, A999–A1004.

58. Du, Y.A., and Holzwarth, N. (2007). Mechanisms of Li+ diffusion in crystalline γ-and β− $Li_3PO_4$ electrolytes from first principles. Phys. Rev. B Condens. Matter Mater. Phys. *76*, 174302.

59. Wert, C., and Zener, C. (1949). Interstitial atomic diffusion coefficients. Phys. Rev. *76*, 1169.

60. Allen, P.B., Feldman, J.L., Fabian, J., and Wooten, F. (1999). Diffusons, locons and propagons: character of atomie yibrations in amorphous Si. Philos. Mag. B *79*, 1715–1731.

61. Li, Z.-P., Mori, T., Zou, J., and Drennan, J. (2012). Optimization of ionic conductivity in solid electrolytes through dopant-dependent defect cluster analysis. Phys. Chem. Chem. Phys. *14*, 8369–8375.

62. Gordiz, K., and Henry, A. (2017). Phonon transport at interfaces between different phases of silicon and germanium. J. Appl. Physiol. *121*, 025102.

63. Seyf, H.R., and Henry, A. (2016). A method for distinguishing between propagons, diffusions, and locons. J. Appl. Physiol. *120*, 025101. https://doi.org/10.1063/1.4955420.

64. Gonzalez-Lafont, A., Truong, T.N., and Truhlar, D.G. (1991). Interpolated variational transition-state theory: practical methods for estimating variational transition-state properties and tunneling contributions to chemical reaction rates from electronic structure calculations. J. Chem. Phys. *95*, 8875–8894.

65. Muy, S., Bachman, J.C., Chang, H.-H., Giordano, L., Maglia, F., Lupart, S., Lamp, P., Zeier, W.G., and Shao-Horn, Y. (2018). Lithium conductivity and Meyer-Neldel rule in $Li_3PO_4$–$Li_3VO_4$–$Li_4GeO_4$ lithium superionic conductors. Chem. Mater. *30*, 5573–5582.

66. de Klerk, N.J.J., van der Maas, E., and Wagemaker, M. (2018). Analysis of diffusion in solid-state electrolytes through MD simulations, improvement of the Li-ion conductivity in β-$Li_3PS_4$ as an example. ACS Appl. Energy Mater. *1*, 3230–3242.

67. Vargas-Barbosa, N.M., and Roling, B. (2020). Dynamic ion correlations in solid and liquid electrolytes: how do they affect charge and mass transport? ChemElectroChem *7*, 367–385.

68. Shiga, T., Shiomi, J., Ma, J., Delaire, O., Radzynski, T., Lusakowski, A., Esfarjani, K., and Chen, G. (2012). Microscopic mechanism of low thermal conductivity in lead telluride. Phys. Rev. B Condens. Matter Mater. Phys. *85*, 155203.

69. Brenner, T.M., Gehrmann, C., Korobko, R., Livneh, T., Egger, D.A., and Yaffe, O. (2020). Anharmonic host-lattice dynamics enable fast ion conduction in superionic AgI. Phys. Rev. Mater. *4*, 115402.

70. Brüesch, P., Pietronero, L., Strässler, S., and Zeller, H. (1977). Brownian motion in a polarizable lattice: Application to superionic conductors. Phys. Rev. B *15*, 4631.

71. Fischer, K., Bilz, H., Haberkorn, R., and Weber, W. (1972). Covalency and deformability of Ag+-ions in the lattice dynamics of silver halides. Phys. Status Solidi B Basic Res. *54*, 285–294.

72. Niedziela, J.L., Bansal, D., May, A.F., Ding, J., Lanigan-Atkins, T., Ehlers, G., Abernathy, D.L., Said, A., and Delaire, O. (2019). Selective breakdown of phonon quasiparticles across superionic transition in $CuCrSe_2$. Nat. Phys. *15*, 73–78.

73. Ding, J., Niedziela, J.L., Bansal, D., Wang, J., He, X., May, A.F., Ehlers, G., Abernathy, D.L., Said, A., Alatas, A., et al. (2020). Anharmonic lattice dynamics and superionic transition in $AgCrSe_2$. Proc. Natl. Acad. Sci. USA *117*, 3930–3937.

74. Bührer, W., Nicklow, R., and Brüesch, P. (1978). Lattice dynamics of β-(silver iodide) by neutron scattering. Phys. Rev. B Condens. Matter *17*, 3362.

75. Zeller, H., Brüesch, P., Pietronero, L., and Strässler, S. (1976). Lattice dynamics and ionic motion in superionic conductors. In Superionic Conductors: Physics of Solids and Liquids, G.D. Mahan and W.L. Roth, eds. (Springer), pp. 201–215.

76. Hull, S. (2004). Superionics: crystal structures and conduction processes. Rep. Prog. Phys. *67*, 1233.

77. Mahan, G. (2013). Superionic Conductors: Physics of Solids and Liquids (Springer).

78. Wang, Y., Richards, W.D., Ong, S.P., Miara, L.J., Kim, J.C., Mo, Y., and Ceder, G. (2015). Design principles for solid-state lithium superionic conductors. Nat. Mater. *14*, 1026–1031.

79. Hartridge, A., Krishna, M.G., and Bhattacharya, A. (1998). Optical constants of nanocrystalline lanthanide-doped ceria thin films with the fluorite structure. J. Phys. Chem. Solids *59*, 859–866.

80. Rokakh, A., Matasov, M., and Zhukov, A. (2010). Spectral control of secondary ion photoeffect: a way to optoionics? Nanotechnol. Russ. *5*, 390–398.

81. Senocrate, A., Kotomin, E., and Maier, J. (2020). On the way to optoionics. Helv. Chim. Acta *103*, e2000073.

82. Kim, K., and Kaviany, M. (2016). Phonocatalysis. An ab initio simulation experiment. AIP Adv. *6*, 065124.

83. Henkelman, G., Uberuaga, B.P., and Jónsson, H. (2000). A climbing image nudged elastic band method for finding saddle points and minimum energy paths. J. Chem. Phys. *113*, 9901–9904.

84. Deng, Y., Eames, C., Chotard, J.N., Lalère, F., Seznec, V., Emge, S., Pecher, O., Grey, C.P., Masquelier, C., and Islam, M.S. (2015). Structural and mechanistic insights into fast lithium-ion conduction in $Li_4SiO_4$–$Li_3PO_4$ solid electrolytes. J. Am. Chem. Soc. *137*, 9136–9145.

85. Islam, M.S., and Fisher, C.A. (2014). Lithium and sodium battery cathode materials: computational insights into voltage, diffusion and nanostructural properties. Chem. Soc. Rev. *43*, 185–204.

86. Lewis, G., and Catlow, C. (1985). Potential models for ionic oxides. J. Phys. C Solid State Phys. *18*, 1149.

87. Todorov, I.T., Smith, W., Trachenko, K., and Dove, M.T. (2006). DL_POLY_3: new dimensions in molecular dynamics simulations via massive parallelism. J. Mater. Chem. *16*, 1911–1918.

88. Pedone, A., Malavasi, G., Menziani, M.C., Cormack, A.N., and Segre, U. (2006). A new

self-consistent empirical interatomic potential model for oxides, silicates, and silica-based glasses. J. Phys. Chem. B *110*, 11780–11795.

89. Wang, B., Chakoumakos, B., Sales, B., Kwak, B., and Bates, J. (1995). Synthesis, crystal structure, and ionic conductivity of a polycrystalline lithium phosphorus oxynitride with the γ-$Li_3PO_4$ structure. J. Solid State Chem. *115*, 313–323.

90. Yakubovich, O., and Urusov, V. (1997). Electron density distribution in lithiophosphatite Li 3 PO 4; crystallochemical features of orthophosphates with hexagonal close packing. Crystallogr. Rep. *42*, 261–268.

91. Zemann, J. (1960). Die kristallstruktur von lithiumphosphat, $Li_3PO_4$. Acta Crystallogr. *13*, 863–867.

92. Gale, J.D. (1997). GULP: A computer program for the symmetry-adapted simulation of solids. J. Chem. Soc. Faraday Trans. *93*, 629–637.

93. Plimpton, S. (1995). Fast parallel algorithms for short-range molecular dynamics. J. Comp. Physiol. *117*, 1–19. https://doi.org/10.1006/jcph.1995.1039.

94. McGaughey, A., and Kaviany, M. (2005). Observation and description of phonon interactions in molecular dynamics simulations. Phys. Rev. B Condens. Matter Mater. Phys. *71*, 184305.

95. Raj, A., and Eapen, J. (2019). Deducing phonon scattering from Normal Mode excitations. Sci. Rep. *9*, 7982.

96. Kubo, R. (1966). The fluctuation-dissipation theorem. Rep. Prog. Phys. *29*, 255.

97. He, X., Zhu, Y., Epstein, A., and Mo, Y. (2018). Statistical variances of diffusional properties from ab initio molecular dynamics simulations. Npj Comput. Mater. *4*, 18.

98. Gordiz, K., Singh, D.J., and Henry, A. (2015). Ensemble averaging vs. time averaging in molecular dynamics simulations of thermal conductivity. J. Appl. Physiol. *117*, 045104.